2020 IEEE International Conference on Robotics and Automation (ICRA)
31 May - 31 August, 2020. Paris, France

Demonstration of Autonomous Nested Search for Local Maxima Using an Unmanned Underwater Vehicle

Andrew Branch[1], James McMahon[2], Guangyu Xu[3], Michael V. Jakuba[4], Christopher R. German[4], Steve Chien[1], James C. Kinsey[4], Andrew D. Bowen[4], Kevin P. Hand[1], Jeffrey S. Seewald[4]

***Abstract*—Ocean Worlds represent one of the best chances for extra-terrestrial life in our solar system. A new mission concept must be developed to explore these oceans. This mission would require traversing the 10s of km thick icy shell and releasing a submersible into the ocean below. During the transit of the icy shell and the exploration of the ocean, the vehicle(s) would be out of contact with Earth for weeks or potentially months at a time. During this time the vehicle must have sufficient autonomy to locate and study scientific targets of interest. One such target of interest is hydrothermal venting. We have previously developed an autonomous nested search method to locate and investigate sources of hydrothermal venting by locating local maxima in hydrothermal vent emissions. In this work we demonstrate this approach on board an OceanServer Iver2 AUV in Chesapeake Bay, MD using simulated sensor data from a hydrothermal plume model. This represents the first step towards the deployment of this approach in conditions analogous to those that we might expect on an Ocean World.**

I. Introduction

At least eight bodies in our solar system are thought to harbor liquid oceans. In some cases, such as Europa and Enceladus, this ocean is perhaps habitable and encased in an icy shell kilometers thick [1]. To explore these oceans a new mission concept must be developed using ice penetrating submersible vehicles. A notional mission concept for such a mission is outlined in Figure 1. This concept contains three main components. A submersible vehicle, an under-ice base station, and a surface relay. Long mission duration – one or more years to transit the icy shell and a one year exploration mission – requires a low power vehicle, limiting the potential instruments on board. The vehicle would ideally travel hundreds or thousands of kilometers from the base station while still being able to return to transmit data through the under-ice base station and back to Earth. When the surface relay does not have line-of-sight to Earth ground stations (approximately 42.5 hours and 33 hours per orbital period of Europa and Enceledus respectively) and when the submersible vehicle is distant from the under-ice base station, no communication with the vehicle would be feasible. The vehicle would also be operating in a significantly more dynamic environment than previous surface operation mission (e.g. Mars rovers), preventing the use of traditional human in the loop operations. Due to these constraints, the vehicle would need to operate fully autonomously for weeks or months at a time. During this exploration mission the vehicle would be required to autonomously locate, detect, and survey specific targets of scientific interest. One potential target of scientific interest is hydrothermal venting. Evidence for hydrothermal venting has been found on one Ocean World, Enceledus [2], [3]. On Earth, these geological phenomena harbor unique ecosystems and are potentially critical to the origin of life. Similar vents on Ocean Worlds could be the best chance at extra-terrestrial life in our Solar System.

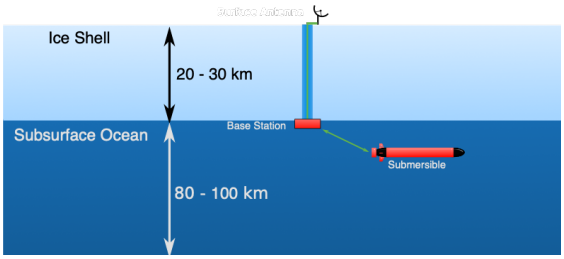

Fig. 1: Notional Europa submersible mission showing the communication pathway from the submersible vehicle to Earth. Approximate ice thickness and ocean depth are labeled.

We have previously developed a fully autonomous nested search strategy for the localization of hydrothermal venting based on a human-in-the-loop three phase nested search commonly used in the field [4], [5]. This work presents a field demonstration of this previously developed fully autonomous search strategy. In June 2019 we deployed an Iver2 AUV in Chesapeake Bay to test this search strategy. As there is no hydrothermal venting in the deployment area, we used simulated data from an FVCOM based hydrothermal plume model [6].

The remainder of the paper is organized as follows. We discuss the structure of hydrothermal venting, the hydrothermal plume model, and our nested search approach. Finally we discuss the experiment, results, and future work.

[1]Jet Propulsion Laboratory, California Institute of Technology, 4800 Oak Grove Dr Pasadena, CA
[2]Code 7130, Physical Acoustics Branch, Naval Research Laboratory, 4555 Overlook Ave SW Washington, DC
[3]Applied Physics Laboratory, University of Washington, 1013 NE 40th St, Seattle, WA
[4]Woods Hole Oceanographic Institution, 266 Woods Hole Rd, Woods Hole, MA

978-1-7281-7395-5/20/$31.00 ©2020 IEEE

Authorized licensed use limited to: Carleton University. Downloaded on September 22,2020 at 01:04:29 UTC from IEEE Xplore. Restrictions apply.

II. Related Work

Adaptive sampling and control of autonomous underwater vehicles has been extensively studied, including foundational work with the Autonomous Ocean Sampling Network [7], [8], [9], [10], [11].

Hydrothermal vent localization on Earth is often done with a non-autonomous three-phase nested search [4]. [12] demonstrates this method in a number of cruises. [13] presents a method to autonomously revisit areas of interest after the primary mission is completed. [14] uses occupancy grid mapping in order to localize vents. [15] uses a trigger based approach in order to gather higher resolution data in areas of strong sensor readings. These three approaches are not fully autonomous and require humans to develop the base mission used.

[16] field tests a strategy inspired by moths in order to trace chemical plumes. [17] and [18] use moth based strategies in order to localize hydrothermal venting. These methods are susceptible to local maxima from plume fluid that detached from the main plume source and can be misled by changes in tidal currents. Our method reduces the issues posed from local maxima and tidal currents by performing coarse surveys over the plume extent before progressively refining regions of high plume concentration, as opposed to following gradients upstream. [19] uses a belief-maximization algorithm to find a target of interest in simulation. Additionally, the above approaches have been tested in idealized plume simulation environments. Our hydrothermal plume simulation provides more realistic plume dynamics for initial testing.

III. Hydrothermal Venting

Hydrothermal venting produces a plume which can be used to locate the source. The structure of the plume is shown in Figure 2. Hydrothermal fluid exiting the vent is less dense than the surrounding water, resulting in the formation of a buoyant plume. Due to entrainment, the plume is continuously diluted by the ambient water column and expands from ~10 cm at the vent source to ~100 m at equilibrium. Upon reaching equilibrium, the plume expands horizontally — ten to hundreds of kilometers — to form the non-buoyant plume [20]. The non-buoyant plume height is a function of the properties of the hydrothermal vent fluid as well as the surrounding water column [21]. In the Pacific the non-buoyant plume is normally observed at 100-150 m above the seafloor, while in the Atlantic it is normally closer to 200-400 m [22].

Hydrothermal plumes are the main source of information when localizing venting. However, tidal flows lead to local maxima [23], turbulent flow disrupting smooth gradients, differing vent types and strengths, and an unknown number of sources increase the difficulty of determining the plume source.

[4] uses three primary sensors in the detection of hydrothermal plumes: temperature, optical backscatter [24], [25], and a chemical sensor such as oxidation-reduction potential [26]. These sensors may be good candidates for inclusion on a submersible mission to an Ocean World due to their compact form factor (100s of grams) and low power consumption (10s of milliwatts).

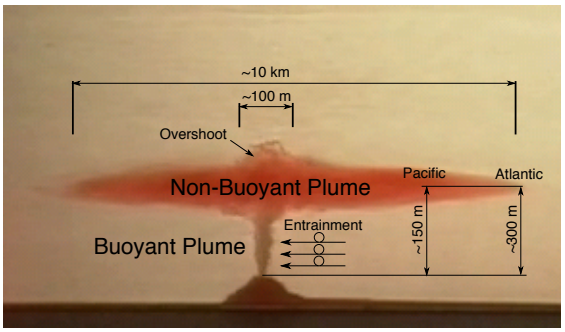

Fig. 2: Demonstration of a hydrothermal plume performed in an aquarium tank. The buoyant and non-buoyant components of the hydrothermal vent plume are labeled with approximate scales. Image courtesy of C. German, WHOI

IV. Hydrothermal Plume Model

A simulation environment was developed using a hydrothermal plume dispersion simulation and a vehicle model. A numerical simulation of hydrothermal plume dispersion is performed using FVCOM [6], an ocean-circulation model, at Axial Seamount on the Juan de Fuca Ridge. The abundant lava supply to Axial supports vigorous hydrothermal systems and frequent volcanic activity, which have drawn extensive on-going scientific research that makes Axial one of the best-studied seamounts on this planet. A snapshot of this simulation is shown in Figure 3. The unstructured grid employed in FVCOM supports grid size variation, therefore, proves efficient for the simulation of motion over a broad range of length scales. In addition, FVCOM supports the use of large-scale ocean circulation and tidal model outputs to drive flow across a broad range of frequencies inside the model domain [27].

Our model domain covers 300 by 300 km, centered on the Axial Seamount caldera and is open to flow across all four sides of that region. Horizontal resolution varies from 200 m within a 10 by 10 km region enclosing Axial's caldera to 10km at the domain's boundary. The vertical dimension has 127 uniformly distributed layers, covering the full water column. This results in a ~12 m layer thickness above Axial's summit. The duration of the simulation is 58 days with model outputs sampled hourly. We add a seafloor heat source of 1 gigawatt at the center (0,0) of the model domain inside Axial's caldera. The model output consists of current, temperature, salinity, and a passive tracer, dye, which is released at the vent source. This tracer has a value range of $[0, 100]$. After 30 days the tracer content in a 20 by 20 km region surrounding the vent source reaches a quasi-steady state. In a 50 by 50 km region surrounding the vent source no quasi-steady state is reached before the end of the simulation. More information about this model can be found in [5].

V. Spatial Nested Search

Given a vehicle's starting location, the goal is to produce a control strategy that results in locating the hydrothermal

Authorized licensed use limited to: Carleton University. Downloaded on September 22,2020 at 01:04:29 UTC from IEEE Xplore. Restrictions apply.

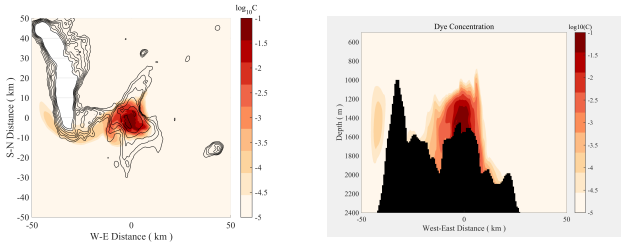

(a) Snapshot taken at 1400m depth (b) W-E transect across the center of the model domain

Fig. 3: Model snapshot taken on Mar 1, 2011 00:00 UTC of the simulated concentration (normalized by the source value) of a neutrally buoyant tracer originating from a hydrothermal vent source of 1 GW heat flux located inside the caldera of Axial Seamount at coordinate center.

vent. The vent is considered found when the region around the vent has been surveyed at a specified resolution. The strategy mimics the field-proven methods of [4]. Due to the limited resolution of the simulation environment, we focus specifically on search in the non-buoyant plume. (The buoyant plume is approximately 100 m, placing it below our 200 m resolution). This corresponds to the ship based CTD casts and — to some extent — phase 1 of the [4] method. Our strategy allows for the localization of plume sources with differing strengths and maintains a robustness to local maxima in vent fluid concentrations and to small scale turbulence. We do this by performing a coarse search over the plume extent and then progressively refine the resolution of surveys in regions of highest plume strength. Before we can search for hydrothermal venting, we must have some method for detecting plumes. Ideally this would involve modeled sensors for temperature, optical backscatter, and oxidation reduction potential. However, currently we only use the passive tracer in the model as a direct measure of the hydrothermal plume. This is an area of future improvement.

The description of the algorithm from [5] is included here. A spiral is initiated at the start location. The horizontal spacing of the spiral is manually selected to be the expected size of the feature, insuring it is seen during this initial survey. During this spiral the vehicle completes vertical profiles through the extent of the water column. When the max plume strength value of a single profile exceeds the specified threshold, $plume_t$ in Algorithm 1, the second phase of surveys begins. The height of the detected feature, p_h, is determined by binning the data from the vertical profile, p_d, at a 10 m resolution and selecting the bin with the largest average value. The subsequent surveys are performed at a depth of p_h.

During the second phase of surveys, the search space is partitioned into bins, $survey\_bins$, of size $spacing_0$. These bins are separated into four quadrants centered on the corner of the bin closest to the location of the plume detection. A dynamic lawnmower survey is executed in each of the four quadrants. The dynamic lawnmower algorithm is outlined in Algorithm 2. The spacing of the lawnmower pattern, $track\_spacing$, is specified beforehand. The direction of the lawnmower pattern is defined by $along\_track$ and $across\_track$. Each track line of the lawnmower pattern consists of sections with length equal to the spacing. At least $min\_sections$ sections are completed per track line. If $sections\_limit$ sections have average plume strengths below $plume_t$ and the sections have monotonically decreasing average plume strengths, then the track line is completed and the next track line is commenced. $min\_sections$ and $sections\_limit$ are manually specified search parameters. If the maximum value of an entire track line is less than $plume_t$ then the current lawnmower survey is ended and the next begins. The data from each dynamic lawnmower is binned into $survey\_bins$.

An example dynamic lawnmower is shown in Figure 4. The plot is subdivided into track line sections. The average plume strength is listed in each section; a green background indicates that the average plume strength is greater than the specified threshold, $plume_t$. Two boundaries to the survey are shown. Upon reaching the right-most boundary, the vehicle completes the current trackline. The boundaries correspond to the shared edges of the four quadrants defined during the search process.

Upon the completion of each dynamic lawnmower, local maxima of $survey\_bins$ are found. A maximum is declared when the 8 neighboring bins of the same resolution have a max plume detection value less than that of the center bin. Once a maximum has been found a nested "lawnmower" survey begins. An example of this process is shown in Figure 5. The local maximum — shown in green — and its neighbors are subdivided into smaller bins with one-third the side length of their parents. A lawnmower with spacing equal to one-third that of the previous lawnmower survey and with track lines centered on each row of nested bins is initiated. The new nested lawnmower survey covers the local maximum and all surrounding neighbors. If any bin has previously been surveyed at the current resolution it will not be surveyed again. If multiple local maxima have been found, they are prioritized on plume strength. This process repeats recursively until a survey spacing of $final\_spacing$, is reached. If no local maxima are found during a dynamic lawnmower, or all local maxima have been exhausted before the survey spacing of $final\_spacing$ is reached, then the dynamic lawnmowers resume. After all dynamic lawnmower surveys are completed the spiral is resumed. Another set of dynamic lawnmowers is started if a plume is detected outside of the previously searched area.

VI. Experiment

A. Vehicle

The vehicle used to demonstrate the autonomous nested search algorithm is an OceanServer Iver2 AUV (see fig.6). The Iver2 AUV is a lightweight vehicle that employs several sensors for navigation and data collection. Specifically, the AUV uses an internal compass, doppler velocity logs (DVL), and GPS receiver to estimate the current position while on the surface (GPS) and underway (compass + DVL). Internally, the AUV is equipped with two computers operating

Authorized licensed use limited to: Carleton University. Downloaded on September 22,2020 at 01:04:29 UTC from IEEE Xplore. Restrictions apply.

Algorithm 1 Autonomous Nested Search

procedure NESTED_SEARCH
  $plans \leftarrow$ empty stack
  $visited \leftarrow$ empty set
  $plans.push(spiral)$
  $survey\_bins \leftarrow$ bins of size $spacing_0$
  while $plans.size > 0$ and not timed out **do**
    Execute or Continue $plans.top()$
    if executing spiral **then**
      Wait until end of vertical profile
      $p_d \leftarrow$ Get data from profile
      $d \leftarrow max(p_d)$
      if $d >= plume_t$ and $d.location$ not explored **then**
        $bins \leftarrow profile\_data$ binned at 10 meters and averaged
        $p_h \leftarrow max(bins).height$
        $(x, y) \leftarrow$ bin corner closest to $d.position$
        $plans.push(dynamic\_lawnmower(x, y, p_h, 90^\circ, 0^\circ, spacing_0))$
        $plans.push(dynamic\_lawnmower(x, y, p_h, -90^\circ, 0^\circ, spacing_0))$
        $plans.push(dynamic\_lawnmower(x, y, p_h, -90^\circ, 180^\circ, spacing_0))$
        $plans.push(dynamic\_lawnmower(x, y, p_h, 90^\circ, 180^\circ, spacing_0))$
        Execute $plans.top()$
    else
      while $plans.top()$ is not completed **do**
        Wait
      $survey\_data \leftarrow$ Get data from latest survey
      $survey\_bins.add\_data(survey\_data)$
      $maxima \leftarrow get\_bin\_maxima(survey\_bins)$
      sort $maxima$
      for bin in $maxima$ **do**
        if bin not in $visited$ **then**
          Partition bin and $bin.neighbors()$
          $visited.add(bin)$
          $plans.push(nested\_lawnmower(bin))$
          break
    while $plans.size > 0$ and $plans.top()$ is complete **do**
      $f \leftarrow plans.pop()$
      if $f.spacing < final\_spacing$ and f contains vent source **then**
        return Success
  return Failure

Algorithm 2 Execute Dynamic Lawnmower

procedure EXECUTE_DYNAMIC_LAWNMOWER(x, y, h , along_track, across_track, track_spacing)
  $start\_x \leftarrow x + cos(along\_track) * track\_spacing/2$
  $start\_y \leftarrow y + sin(across\_track) * track\_spacing/2$
  Go to $(start\_x, start\_y, h)$
  $curr\_track \leftarrow 0$
  $curr\_section \leftarrow 0$
  $completed \leftarrow False$
  $section\_data \leftarrow$ empty list
  Start current track line on heading $along\_track$
  while not $completed$ **do**
    Do next section on current track
    $section\_data[curr\_section] \leftarrow$ Get data from last section
    $curr\_section \leftarrow curr\_section + 1$
    if $curr\_section >= min\_sections$ or survey boundary reached **then**
      if $avg(section\_data[i]) < plume_t$ for last $sections\_limit$ sections and monotonically decreasing **then**
        $curr\_track \leftarrow curr\_track + 1$
        if $max(section\_data) < plume\_thresh$ **then**
          $completed \leftarrow True$
          $section\_data \leftarrow$ empty list
          Travel $track\_spacing$ on heading $across\_track$
          if $curr\_track$ is even **then**
            Start next track line on heading $along\_track$
          else
            Start next track line on heading $-along\_track$

in a *frontseat-backseat* configuration. The frontseat, a main vehicle computer developed by OceanServer, controls the actuation of the vehicle and generates the navigation solution (Geodesic coordinates, heading, speed, depth/altitude). The backseat computer is built in-house and runs the MOOS-IvP autonomy architecture onboard a PC104 stack running Ubuntu 18.04 on an Intel Core-i7 (2.4 GHz) with 4 GB of RAM. The architecture of the autonomy system leverages MOOS-IvP to handle the passing of data between different processes and to arbitrate several behaviors in order to generate a desired navigation solution (Heading, Depth, and Speed).

In this work we add two main components to MOOS-IvP: (i) The Nested Search Planner application, and (ii) the FVCOM plume simulator app (see fig.7). The navigation solution generated by the frontseat is passed through to both the planning and simulator app. Simulated sensor readings from the FVCOM simulation are also passed forward to the planning application which then generates updated plans for the IvP Helm to follow throughout the course of the mission. IvP Helm then arbitrates between safety behaviors (battery monitoring, region monitoring, etc.) and waypoints that define the nested search plan resulting in the desired heading, depth, and speed.

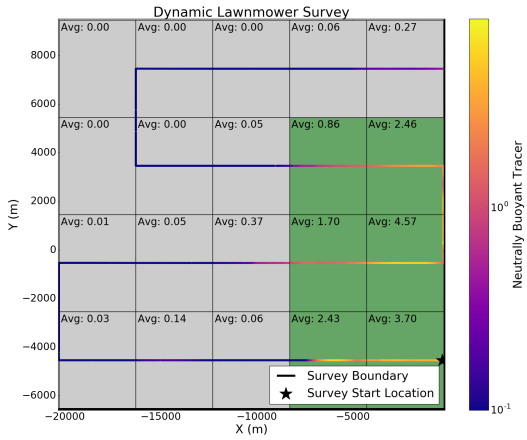

Fig. 4: Plot showing an example dynamic lawnmower survey. The survey area is partitioned into regions representing sections of each track line. Regions shaded green have an average plume strength over the specified threshold. The average value is labeled in the upper left corner of each region. The two survey boundaries are shown as thick black lines on the right and bottom of the plot. The starting location is marked with a black star.

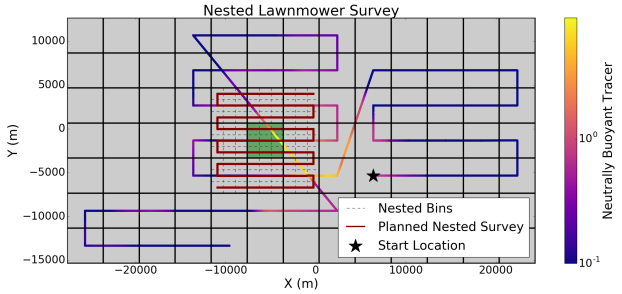

Fig. 5: Example of the planning process for the nested lawnmower search. The search space is divided into square bins with sides equal to the lawnmower spacing. Upon finding a local maximum bin, the bin and all its neighbors are subdivided into nested bins of one-third the side length. A lawnmower pattern is then executed such that each track line is centered on a row of bins. The vehicle path and observed tracer is plotted. The planned nested lawnmower is show in dark red. The starting location is marked with a black star. Note that the measured passive tracer does not remain the same on subsequent measurements of the same location due to the temporal variation in fluid concentrations.

B. Mission Setup

Two operational constraints required the modification of the hydrothermal model, vehicle endurance and water depth. The Iver2 AUV used in the experiment has an endurance of 25-30 km. This is not sufficient for a convincing test of the nested bin search given the size of the hydrothermal plume model. To compensate for this, the model was scaled in the xy direction by a factor of 1/8, resulting in a model resolution of 25m. An experiment area of 1.5 km by 1.5 km was also defined to focus the search and prevent the vehicle from travelling too far from the shore. The water depth in this experiment region was approximately 7 meters deep.

Authorized licensed use limited to: Carleton University. Downloaded on September 22,2020 at 01:04:29 UTC from IEEE Xplore. Restrictions apply.

Fig. 6: Iver2 AUV parked on the shore at NRL's Chesapeake Beach Detachment after performing an experiment.

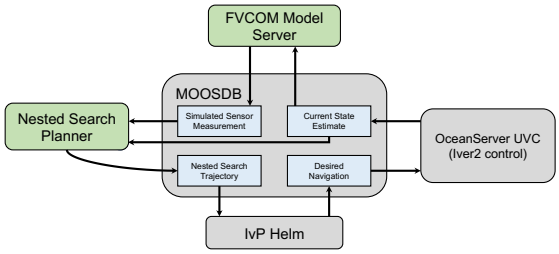

Fig. 7: Simplified version of the autonomy architecture showing the main components required for autonomous nested search using an OceanServer Iver2 AUV.

As the original hydrothermal plume model is approximately 1400 meters deep at the vent site it could clearly not be used in this form. In addition the bathymetry of the model seafloor is not as flat at the experiment operation region. To compensation for this we removed the portion of the model in the vertical direction that contains no hydrothermal plume and uniformly selected 9 layers from the remaining portion of the model. This resulted in a modified model with 9 layers with a 0.66 meter layer size, for a total of 6 meters of vertical depth. We also gave the model a flat seabed by making the layers of uniform height. This resulted in a model that fit in our experiment region and with a vertical resolution within the vehicles ability to maintain depth. We do note that this extreme modification of the model is not ideal. However, visual inspection of the resulting model shows that the important features for our particular algorithm are still present (multiple local maxima and varying plume strength with depth). The goal of this experiment was to demonstrate the algorithm running on board an AUV and prepare for deployments without a plume model. The results of the modification of the model can be seen in Figure 8. Analysis in simulation of the search method can be found here, [5].

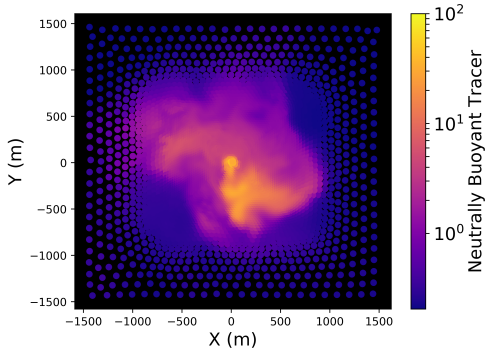

Fig. 8: Snapshot taken at 7 m depth of the modified hydrothermal plume model. The plume concentration is plotted in the form of the neutrally buoyant tracer. At this depth we see the largest plume dispersion.

We deployed the AUV from shore each day from June 4th to June 7th. The profile of a single run is as follows. The vehicle traversed near the surface to the target experiment region, performed the autonomous nested search described previously then returned to the shore for recovery. The resolution of the spiral and initial lawnmowers was set to 200m and 150m respectively, with a final survey goal of 25m, the same resolution as the modified hydrothermal plume model. If the vehicle was unable to locate the hydrothermal vent before a specified timeout it would return to shore. The vehicle maintained accurate localization by surfacing every 10 minutes for a GPS fix. Each day the location of the hydrothermal vent and the starting location of the vehicle was set. The location of the hydrothermal plume was modified by moving the origin of the model in the experiment region. In total we performed 5 runs on the vehicle. We always start the vehicle south of the hydrothermal vent. Due to the design of the algorithm, this results in shorter distances travelled and allowed us to better demonstrate the search algorithm while remaining within the vehicle's endurance.

VII. Results

A total of 5 runs were run over the 4 days of the experiment. On the first day, 2 runs were performed with the primary goal of testing the interface between the nested search planner. There were no issues with the interface between the planner, the model, and the vehicle. The primary goal of all subsequent runs was to demonstrate the nested search planner. The experiment region was set to 1.5 by 1.5 kilometers and the run timeout was set to 3.5 hours. These parameters ensure that the vehicle has the opportunity to demonstrate the nested search algorithm while still returning to the shore before the end of the vehicles endurance. On the day 2 run, Figure 9, we see intermittent data sampled from the model. The search algorithm selected the height of the lawnmower surveys to be at the bottom of the model. As the vehicle is not able to perfectly hold depth it was periodically at a depth lower than the model, resulting in no valid data. There is also a known issue with this methods performance, as currently implemented, when searching in the death direction. The depth at which all lawnmower surveys are performed in determined only once during the initial contact with the plume. As the plume depth varies based on water density and location, the vehicle is not guaranteed to maintain contact with the strongest depth band of the plume throughout the search. This can result in failure to identify the plume source. For the purposes of the remaining runs in this demonstrations, the depth at which the lawnmower surveys were performed was fixed to be roughly the center of the plume. In future iterations we want to improve the search algorithm to also search in the depth direction throughout the entire run to maintain contact with the plume.

Authorized licensed use limited to: Carleton University. Downloaded on September 22,2020 at 01:04:29 UTC from IEEE Xplore. Restrictions apply.

During all runs we see similar behavior. The vehicle performs a spiral until contacting the plume, then perform the dynamic lawnmower behavior until a local maximum is seen, finally they perform nested lawnmower surveys at subsequent local maxima until the final survey size is reached.

The day 2 run can be seen in Figure 9 and the day 3 (top) and day 4 (bottom) runs can be seen in Figure 10. The day 4 run resulted in the most interesting demonstration. We see the vehicle performing the dynamic lawnmower then transitioning to the nested survey. The largest maximum seen at this point is south of the hydrothermal vent location, resulting in a nested lawnmower survey that does not cover the vent location. Upon completion, this lawnmower survey is extended further north to cover an additional local maximum that is co-located with the vent site. This behavior is expected in real operations due multiple local maxima in the plume that are not associated with the vent location.

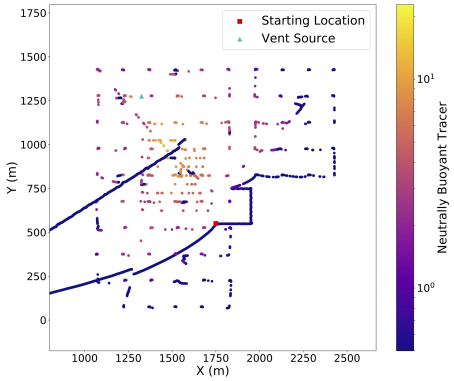

Fig. 9: Day 2 Run. Sensed plume strength is plotted.

VIII. Future Work

The primary future work to be completed is full real world testing at a hydrothermal venting site. In addition to more testing, the algorithm can be improved in a number of ways. The lawnmower surveys can be improved to guarantee closing contours for local maxima, the search can include a depth component through the duration of the run, temporal variation in the plume from should be accounted for, and other search strategies should be developed for comparison.

This work was originally developed for the localization of hydrothermal venting. However, as the search operates by locating local maxima, a similar approach could be applied in other underwater vehicle search problems. The approach could be applied to any oceanographic measure such as temperature, salinity, chlorophyll, or other chemical sensors. An additional application is acoustic source localization. Given some acoustic source determine the location of that source based on the strength of the received sound wave. Adaptations of this algorithm for other uses will also expand the potential for real world experiments.

Hydrothermal venting is not the only target of interest. While not all ocean processes on Earth are expected to recur on other ocean worlds distant from the sun, the following can

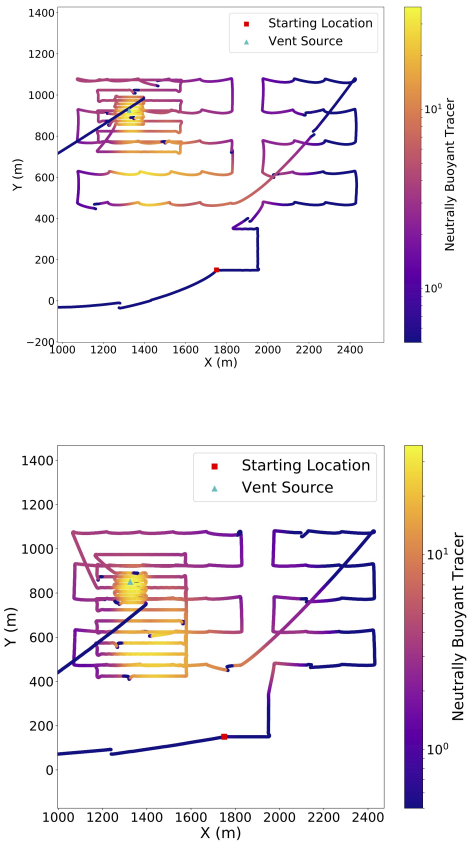

Fig. 10: (top) Day 3 run. (bottom) Day 4 run. Sensed plume strength is plotted.

be explored for their applications to Ocean Worlds: thermoclines [28], [29], [30], ocean fronts [31], [32], algal bloom patch [33], [34], [35], [36], and submesoscale structures [37].

Autonomous science is only one autonomy task required by an ocean worlds submersible. The vehicle would also be required to handle resource constraints, selectively choose which data to transmit back to Earth over the limited bandwidth, and perform underwater navigation.

IX. Conclusion

We demonstrated an autonomous nested search method for hydrothermal venting, based on a field tested manual three-phase search approach [4]. We deployed an OceanServer Iver2 AUV into Chesapeake Bay, MD running the nested search method on board as well as a hydrothermal plume model to simulate the required sensor data. Over a 1 week period we ran 5 mission on board the vehicle demonstrating the performance of the algorithm.

Acknowledgment

Portions of this work were performed by the Jet Propulsion Laboratory, California Institute of Technology, under contract with the National Aeronautics and Space Administration. Portions of this work were funded by the Naval Research Laboratory and Woods Hole Oceanographic Institution.

Authorized licensed use limited to: Carleton University. Downloaded on September 22,2020 at 01:04:29 UTC from IEEE Xplore. Restrictions apply.

REFERENCES

[1] National Aeronautics and Space Administration. (2018) Ocean worlds. [Online]. Available: https://www.nasa.gov/specials/ocean-worlds

[2] H.-W. Hsu, F. Postberg, Y. Sekine, T. Shibuya, S. Kempf, M. Horányi, A. Juhász, N. Altobelli, K. Suzuki, Y. Masaki, *et al.*, "Ongoing hydrothermal activities within enceladus," *Nature*, vol. 519, no. 7542, p. 207, 2015.

[3] J. H. Waite, C. R. Glein, R. S. Perryman, B. D. Teolis, B. A. Magee, G. Miller, J. Grimes, M. E. Perry, K. E. Miller, A. Bouquet, J. I. Lunine, T. Brockwell, and S. J. Bolton, "Cassini finds molecular hydrogen in the enceladus plume: Evidence for hydrothermal processes," *Science*, vol. 356, no. 6334, pp. 155–159, 2017. [Online]. Available: http://science.sciencemag.org/content/356/6334/155

[4] C. R. German, D. R. Yoerger, M. Jakuba, T. M. Shank, C. H. Langmuir, and K.-i. Nakamura, "Hydrothermal exploration with the autonomous benthic explorer," *Deep Sea Research Part I: Oceanographic Research Papers*, vol. 55, no. 2, pp. 203–219, 2008.

[5] A. Branch, G. Xu, M. V. Jakuba, C. R. German, S. Chien, J. C. Kinsey, A. D. Bowen, K. P. Hand, and J. S. Seewald, "Autonomous nested search for hydrothermal venting," in *Workshop on Planning and Robotics, International Conference on Automated Planning and Scheduling (ICAPS PlanRob 2018)*, Delft, Netherlands, June 2018. [Online]. Available: https://ai.jpl.nasa.gov/public/papers/branch_planrob2018_hydrothermal.pdf

[6] C. Chen, H. Liu, and R. C. Beardsley, "An unstructured grid, finite-volume, three-dimensional, primitive equations ocean model: Application to coastal ocean and estuaries," *Journal of Atmospheric and Oceanic Technology*, vol. 20, no. 1, pp. 159–186, 2003. [Online]. Available: https://doi.org/10.1175/1520-0426(2003)020¡0159:AUGFVT¿2.0.CO;2

[7] T. B. Curtin, J. G. Bellingham, J. Catipovic, and D. Webb, "Autonomous oceanographic sampling networks," *Oceanography*, vol. 6, no. 3, pp. 86–94, 1993. [Online]. Available: http://www.jstor.org/stable/43924649

[8] T. B. Curtin and J. G. Bellingham, "Progress toward autonomous ocean sampling networks," *Deep Sea Research Part II: Topical Studies in Oceanography*, vol. 56, no. 3, pp. 62 – 67, 2009, aOSN II: The Science and Technology of an Autonomous Ocean Sampling Network. [Online]. Available: http://www.sciencedirect.com/science/article/pii/S0967064508002531

[9] S. Ramp, R. Davis, N. Leonard, I. Shulman, Y. Chao, A. Robinson, J. Marsden, P. Lermusiaux, D. Fratantoni, J. Paduan, F. Chavez, F. Bahr, S. Liang, W. Leslie, and Z. Li, "Preparing to predict: The second autonomous ocean sampling network (aosn-ii) experiment in the monterey bay," *Deep Sea Research Part II: Topical Studies in Oceanography*, vol. 56, no. 3, pp. 68 – 86, 2009, aOSN II: The Science and Technology of an Autonomous Ocean Sampling Network. [Online]. Available: http://www.sciencedirect.com/science/article/pii/S0967064508002609

[10] P. Haley, P. Lermusiaux, A. Robinson, W. Leslie, O. Logoutov, G. Cossarini, X. Liang, P. Moreno, S. Ramp, J. Doyle, J. Bellingham, F. Chavez, and S. Johnston, "Forecasting and reanalysis in the monterey bay/california current region for the autonomous ocean sampling network-ii experiment," *Deep Sea Research Part II: Topical Studies in Oceanography*, vol. 56, no. 3, pp. 127 – 148, 2009, aOSN II: The Science and Technology of an Autonomous Ocean Sampling Network. [Online]. Available: http://www.sciencedirect.com/science/article/pii/S0967064508002634

[11] N. E. Leonard, D. A. Paley, F. Lekien, R. Sepulchre, D. M. Fratantoni, and R. E. Davis, "Collective motion, sensor networks, and ocean sampling," *Proceedings of the IEEE*, vol. 95, no. 1, pp. 48–74, Jan 2007.

[12] D. R. Yoerger, A. M. Bradley, M. Jakuba, M. A. Tivey, C. R. German, T. M. Shank, and R. W. Embley, "Mid-ocean ridge exploration with an autonomous underwater vehicle," *Oceanography*, vol. 20, no. 4, pp. 52–61, 2007.

[13] D. R. Yoerger, M. Jakuba, A. M. Bradley, and B. Bingham, "Techniques for deep sea near bottom survey using an autonomous underwater vehicle," *The International Journal of Robotics Research*, vol. 26, no. 1, pp. 41–54, 2007.

[14] M. Jakuba and D. R. Yoerger, "Autonomous search for hydrothermal vent fields with occupancy grid maps," in *Proc. of ACRA*, vol. 8, 2008, p. 2008.

[15] G. Ferri, M. V. Jakuba, and D. R. Yoerger, "A novel trigger-based method for hydrothermal vents prospecting using an autonomous underwater robot," *Autonomous Robots*, vol. 29, no. 1, pp. 67–83, 2010.

[16] J. A. Farrell, S. Pang, and W. Li, "Chemical plume tracing via an autonomous underwater vehicle," *IEEE Journal of Oceanic Engineering*, vol. 30, no. 2, pp. 428–442, 2005.

[17] S. Pang, "Plume source localization for auv based autonomous hydrothermal vent discovery," in *OCEANS 2010*. IEEE, 2010, pp. 1–8.

[18] Y. Tian, A. Zhang, W. Li, J. Yu, Y. Li, and J. Zeng, "A behavior-based planning strategy for deep-sea hydrothermal plume tracing with autonomous underwater vehicles," in *OCEANS 2014-TAIPEI*. IEEE, 2014, pp. 1–10.

[19] Z. Saigol, R. Dearden, J. Wyatt, and B. Murton, "Belief change maximisation for hydrothermal vent hunting using occupancy grids," in *Proceedings of the Eleventh Conference Towards Autonomous Robotic Systems (TAROS-10)*, 2010, pp. 247–254.

[20] C. German and W. Seyfried, "Hydrothermal processes," *Treatise on geochemistry*, vol. 8, pp. 191–233, 2014.

[21] J. S. Turner, *Buoyancy effects in fluids*. Cambridge University Press, 1979.

[22] K. G. Speer and P. A. Rona, "A model of an atlantic and pacific hydrothermal plume," *Journal of Geophysical Research: Oceans*, vol. 94, no. C5, pp. 6213–6220, 1989.

[23] S. R. Veirs, "Heat flux and hydrography at a submarine volcano: Observations and models of the main endeavour vent field in the northeast pacific," Ph.D. dissertation, University of Washington, 2003.

[24] E. T. Baker, C. R. German, and H. Elderfield, "Hydrothermal plumes over spreading-center axes: Global distributions and geological inferences," *Seafloor hydrothermal systems: Physical, chemical, biological, and geological interactions*, pp. 47–71, 1995.

[25] E. T. Baker and C. R. German, "On the global distribution of hydrothermal vent fields," *Mid-ocean ridges*, pp. 245–266, 2004.

[26] K. Nakamura, S. Veirs, C. P. Sarason, R. E. McDuff, F. Stahr, D. R. Yoerger, and A. M. Bradley, "Electrochemical signals in rising buoyant plumes and tidally oscillating plumes at the main endeavour vent field, juan de fuca ridge," *EOS, Transactions of the American Geophysical Union*, vol. 81, no. 48, 2000.

[27] L. Zheng and R. H. Weisberg, "Modeling the west florida coastal ocean by downscaling from the deep ocean, across the continental shelf and into the estuaries," *Ocean Modelling*, vol. 48, pp. 10 – 29, 2012. [Online]. Available: http://www.sciencedirect.com/science/article/pii/S1463500312000327

[28] N. A. Cruz and A. C. Matos, "Adaptive sampling of thermoclines with autonomous underwater vehicles," in *OCEANS 2010*. IEEE, 2010, pp. 1–6.

[29] Y. Zhang, J. G. Bellingham, M. Godin, J. P. Ryan, R. S. McEwen, B. Kieft, B. Hobson, and T. Hoover, "Thermocline tracking based on peak-gradient detection by an autonomous underwater vehicle," in *OCEANS 2010*. IEEE, 2010, pp. 1–4.

[30] L. Sun, Y. Li, S. Yan, J. Wang, and Z. Chen, "Thermocline tracking using a portable autonomous underwater vehicle based on adaptive threshold," in *OCEANS 2016-Shanghai*. IEEE, 2016, pp. 1–4.

[31] A. Branch, M. M. Flexas, B. Claus, E. B. Clark, A. F. Thompson, S. Chien, J. C. Kinsey, D. M. Fratantoni, Y. Zhang, B. Kieft, B. Hobson, and F. P. Chavez, "Front delineation and tracking with multiple underwater vehicles," *J. Field Robotics*, p. submitted, 2018.

[32] N. A. Cruz and A. C. Matos, "Autonomous tracking of a horizontal boundary," in *Oceans-St. John's, 2014*. IEEE, 2014, pp. 1–6.

[33] M. A. Godin, Y. Zhang, J. P. Ryan, T. T. Hoover, and J. G. Bellingham, "Phytoplankton bloom patch center localization by the tethys autonomous underwater vehicle," in *OCEANS'11 MTS/IEEE KONA*, Sept 2011, pp. 1–6.

[34] D. Magazzeni, F. Py, M. Fox, D. Long, and K. Rajan, "Policy learning for autonomous feature tracking," *Autonomous Robots*, vol. 37, no. 1, pp. 47–69, Jun 2014. [Online]. Available: https://doi.org/10.1007/s10514-013-9375-7

[35] J. Das, F. Py, T. Maughan, T. OReilly, M. Messié, J. Ryan, G. S. Sukhatme, and K. Rajan, "Coordinated sampling of dynamic oceanographic features with underwater vehicles and drifters," *The International Journal of Robotics Research*, vol. 31, no. 5, pp. 626–646, 2012.

[36] S. Petillo, H. Schmidt, and A. Balasuriya, "Constructing a distributed auv network for underwater plume-tracking operations," *International Journal of Distributed Sensor Networks*, vol. 2012, pp. Article ID 191 235, 12pp, 2012.

Authorized licensed use limited to: Carleton University. Downloaded on September 22,2020 at 01:04:29 UTC from IEEE Xplore. Restrictions apply.

[37] M. M. Flexas, M. I. Troesch, S. Chien, A. F. Thompson, S. Chu, A. Branch, J. D. Farrara, and Y. Chao, "Autonomous sampling of ocean submesoscale fronts with ocean gliders and numerical model forecasting," *Journal of Atmospheric and Oceanic Technology*, vol. 35, no. 3, pp. 503–521, 2018. [Online]. Available: https://doi.org/10.1175/JTECH-D-17-0037.1

Authorized licensed use limited to: Carleton University. Downloaded on September 22,2020 at 01:04:29 UTC from IEEE Xplore. Restrictions apply.